Materials and Design 112 (2016) 479–484

Contents lists available at ScienceDirect

Materials and Design

journal homepage: www.elsevier.com/locate/matdes

The role of amorphous precursor in phase selection hierarchy in marginal metallic glasses

C. Yildirim [a], M. Kutsal [a], R.T. Ott [b], M.F. Besser [b], M.J. Kramer [b], Y.E. Kalay [a,*]

[a] Department of Metallurgical and Materials Engineering, METU, Ankara 06800, Turkey
[b] Ames Laboratory (DOE), Ames, IA 50011, USA

HIGHLIGHTS

- Different MRO structure were detected in metallic glasses produced using different techniques.
- Metallic glasses having the same chemistry devitrifies to different crystals.
- High number density of nanocrystals are formed by subsequent devitrification of metallic glasses.

GRAPHICAL ABSTRACT

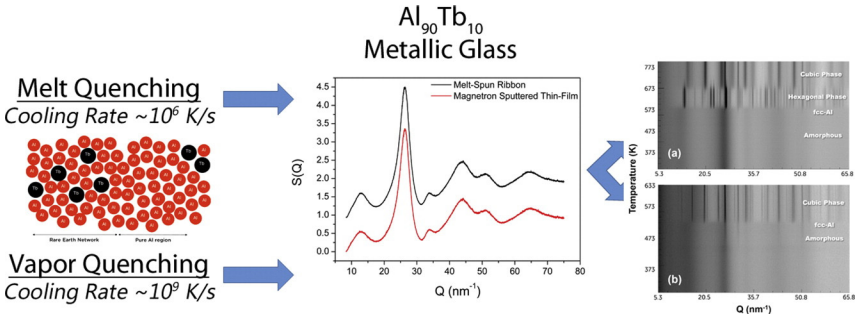

ARTICLE INFO

Article history:
Received 21 May 2016
Received in revised form 8 September 2016
Accepted 16 September 2016
Available online 22 September 2016

Keywords:
Phase selection
Medium-range order
Nanocrystallization
Marginal metallic glass

ABSTRACT

The solid state amorphous structure and devitrification products of $Al_{90}Tb_{10}$ alloys produced by Cu block melt-spinning and magnetron sputtering were investigated by a combined study of differential scanning calorimetry, in-situ X-ray diffraction and conventional transmission electron microscopy. The as-prepared specimens were found to be fully amorphous according to the electron and X-ray diffraction. The thermal analysis and in-situ XRD analyses of the amorphous samples having the same chemistry but different processing history showed clear differences in the devitrification pathways in terms of nanocrystal population, size and the phase selection. The variations in the crystallization path were explained on the basis of distinct topological and chemical medium range ordering observed in as-quenched and as-sputtered amorphous structures.

1. Introduction

Aluminum based marginal glass-forming alloys, Al-RE, Al-TM-RE (RE: rare-earth element; TM: transition metals), comprise an important family of metallic glasses due to their ability of forming of high number density of fcc-Al nanocrystals upon devitrification [1–3]. The high-density of fcc-Al nanocrystals embedded in amorphous matrix can lead to significant increase in mechanical strength in partially devitrified condition [4–8]. As marginal glass-formers need higher cooling rates as compared to conventional metallic glasses, much higher cooling rates on the order of 10^5–10^6 K/s is required. Among vast varieties of techniques, melt-spinning and magnetron sputtering are well established processes to reach higher cooling rates. In melt-spinning process, the molten metal is ejected onto a rotating copper wheel [9] on the other hand in magnetron sputtering the metal is coated onto a cooled Si substrate by the bombardments of ions to the target surface [10]. As its name implies, in melt-spinning glass solidifies from metallic melt, yet in magnetron sputtering glass forms via condensation of the metallic vapor.

* Corresponding author.
E-mail address: ekalay@metu.edu.tr (Y.E. Kalay).

http://dx.doi.org/10.1016/j.matdes.2016.09.060
0264-1275/

Although these systems have been extensively studied, a complete explanation of the underlying nucleation mechanism resulting in a nanocomposite structure with 10^{21-24} m^{-3} nuclei embedded in an amorphous matrix is still lacking. Several hypothesis, such as "quenched-in nuclei" [11,12], "phase separation in amorphous state" [13] have been previously proposed, however they do not explain the totality of the experimental observations. A more recent study on the short to medium-range ordering offers a different perspective by taking into account the topological ordering in the liquid state in Al-Tb system [14]. It was reported that high number density of Al clusters in as-quenched states are inherited from the liquid state prior to quenching the melt, caused by Tb atoms attracting Al atoms in the first shell neighborhood, thus forming a continuous network. Upon rapid solidification, these chemically isolated regions are retained in the amorphous matrix with isolated regions of nearly pure Al, which act as nucleating sites for fcc-Al during devitrification [14]. In another recent study, the existence of such nanoscale amorphous regions, although larger in size, was also confirmed by atom probe tomography (APT) in Al-Y-Fe [15].

In this study we report the role of the short-to-medium range atomic order of the amorphous precursor structure on devitrification behavior of $Al_{90}Tb_{10}$ amorphous alloys. The amorphous and partially crystallized states have been investigated for samples that were produced by two different processes, namely melt spinning and magnetron sputtering. Differences in the thermal devitrification behavior for glasses of same overall composition have been characterized with differential scanning calorimetry (DSC), in-situ x-ray diffraction and transmission electron microscopy (TEM).

2. Experimental procedure

Amorphous ribbons of $Al_{90}Tb_{10}$ with 25 μm thickness and 1.2 mm width were produced by a single copper block melt spinner, quenching from 1423 K at a tangential wheel speed of 30 m/s. The ingots were prepared in a copper-hearth electric arc melting in an argon atmosphere and re-melted three times to ensure compositional homogeneity. Amorphous $Al_{90}Tb_{10}$ thin films with 10 μm thickness were produced by DC magnetron sputtering onto a liquid nitrogen cooled Si wafer. The chemical compositions of as-quenched and as-sputtered alloys were confirmed by electron spectroscopy. EDS indicated 90.3 and 90.6 at.% aluminum for the melt-spun ribbon (as an average of wheel and air sides) and sputtered thin films, respectively. Differential scanning calorimetry (DSC) experiments were conducted using SEIKO SII X-DSC7000. In DSC experiments, approximately 7 to 10 mg of ribbon or sputtered thin-films were filled in Al pans and covered with Al lids, and heated-up from room temperature to 600 K at 10 and 40 K/min under a protective N_2 gas atmosphere. After each scan, an empty pan was placed into the instrument for baseline correction. The isochronal annealing for transmission electron microscopy (TEM) investigations were performed using the same calorimeter with the identical experimental conditions in which DSC traces were obtained. Conventional TEM analyses were conducted using JEOL JEM2100F (at METU) field emission STEM at 200 keV. Specimens for TEM analyses were prepared using electropolishing with a solution of 25 vol.% nitric acid and 75 vol.% methanol at 241 K. In-situ X-ray diffraction experiments were carried out at BL04-MSPD beamline of ALBA Synchrotron Light Laboratory. A double Si monochromator was used to select the wavelength of 0.04136 nm. For room temperature experiments, free-standing samples were attached such that the incoming beam hit the sample surface, inclined with 45°. The diffraction data were collected in the Q-range ($Q = 4\pi\sin(\theta)/\lambda$) where θ is the Bragg's angle and λ is the wavelength of X-ray radiation) of 8.3–75 nm^{-1} using a Mythen array detector system. Melt-spun ribbons and sputtered films were cut by a razor blade and filled into X-ray transparent capillaries having 0.5 mm diameter and 10 μm wall thicknesses. The capillaries were heated from room temperature to 633 K for the sputtered thin-films and to 773 K for the melt-spun ribbons using a hot air blower placed beneath at a constant heating rate of 10 K/min. The temperature of the samples was measured using the thermocouples placed right before the exit of the blower having ±2 K tolerance. Capillaries were heated continuously with the given heating rate and diffraction data were collected in every 3 s within the Q-range of 5.3–65.8 nm^{-1}. Intensity versus Bragg angle data of both samples were first were corrected for background, polarization, absorption, multiple, Compton scattering and then converted to total X-ray structure factor using pdfgetX3 software [16].

3. Results and discussion

Fig. 1(a) shows the total X-ray structure factors (S(Q)) collected at room temperature for the melt-spun and sputtered samples. The amorphous nature of the as-quenched ribbon and as-sputtered thin-film is clearly observed. There are strong pre-peak and side-peak reflections at wave momentum of approximately 13 and 34 nm^{-1} in ribbon specimens. The existence of such additional reflections with relatively robust intensities was previously associated to RE-Al interactions [14,17,18]. The strong atomic coupling between the RE and Al atom results in a selective accumulation of Al atoms around the Tb, which persists in molten state [19]. The average measured coordination number around Tb atoms was found to be 15 using ab-initio constrained RMC simulations, which approximately corresponds to 91% Al in the first shell neighborhood [14]. The presence of Tb atoms with such a high coordination of Al causes the amorphous matrix to be divided into Al-rich and Al-depleted regions. These Al-rich regions were found to be the origin of highly populated fcc-Al nanocrystallization upon devitrification whereas; Al-depleted regions inhibit long-range diffusion and restrict the size of individual fcc-Al nanocrystals to stay less than 50 nm. The selected-area diffraction (SAD) patterns collected from the melt-spun ribbons and the sputtered thin-films of $Al_{90}Tb_{10}$ indicate a fully amorphous structure (Fig. 1(b) and (c)). The total X-ray structure factors, on the other hand, reveal similar pre-peak and side-peak formation at almost exactly the same position with relatively low intensities, as shown in Fig. 1(a). The full-width at half-maximum values calculated by Lorentzian approximation indicated a broader peak for the magnetron sputtered thin-films. The structure related values are tabulated in Table 1. Similar trend was previously observed between the melt-spun $Al_{90}Tb_{10}$ ribbon and its molten state [14]. The existence of such pre-peak was associated with the existence of highly-populated Al-RE interactions [10,13–15,17]. The increase in such interactions drives the

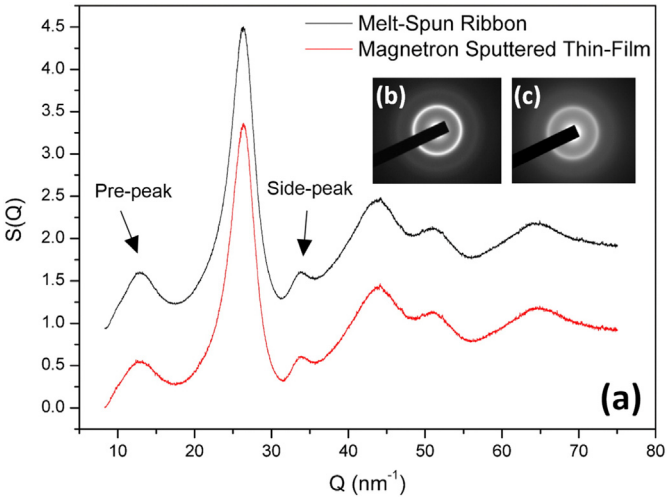

Fig. 1. (a) Room temperature total X-ray structure factors (S(Q)) of melt-spun ribbons (black) and sputtered thin-films (red) of $Al_{90}Tb_{10}$. (b) and (c) SAD patterns of melt-spun ribbons and sputtered thin-films of $Al_{90}Tb_{10}$ at room temperature, respectively. (For interpretation of the references in color in this figure legend, the reader is referred to the web version of this article). (For interpretation of the references to color in this figure legend, the reader is referred to the web version of this article.)